NUMERICAL STUDY OF MODEL AND WALL INTERFERENCE IN A SUPERSONIC WIND TUNNEL

초음속 풍동내에서의 모델과 벽면 간섭에 관한 수치적 연구

S. K. Hong[1], H. K. Ahn[2]
홍 승 규[1], 안 효 근[2]

초 록

마하수 4일때 초음속 풍동의 벽면과 모델지지부의 간섭에 관해 연구하였다. 특히 모델지지부 주위에서의 충격파 형성과 sting, strut 그리고 second throat에서의 반사 충격파의 상호 작용에 연구의 촛점을 두었다. 수치 기법은 내재적 플럭스 차분 분할기법 (implicit flux-difference splitting technique)을 사용하였다.

2차원과 3차원 유동해석 결과로 부터 모델지지부 후류의 유동에 미치는 diffuser 출구 경계조건의 영향을 알아보았다.

1. Introduction

Current paper describes mainly a numerical effort to simulate the flowfield within an ADD wind tunnel at Mach 4. The model is a rather long axisymmetric projectile placed in the rectangular wind tunnel with a test section of 4^{ft} by 4^{ft}. The flow condition is such that Po = 200(psia) , M = 4, model length = 4^{ft}. Although the wind tunnel wall and the model are three-dimensional in reality, the problem is simplified to a two-dimensional problem at first by smoothing out the mid-plane of the flow domain. The fully three-dimensional study is undertaken by simulating the model, sting, model support, vertical strut and the insert as best as we can model them along with the varying cross-sectional areas inside the tunnel.

Instead of setting the pressure boundary conditions at the outflow plane, the computational domain is chosen from nozzle throat to end of the diffuser, far downstream of the model support area in the case of two-dimensional study. For 3-D case, due to the increase in the number of grid points, the computational domain is not extended as far downstream as in the 2-D case, but includes all the parts attached to the test model. Some pertinent investigations were done earlier to simulate mainly the starting process within a hypersonic wind tunnel[1], capturing the shock interactions with upwind TVD schemes. The current work in contrast concentrates on the steady-state flow pattern over the model support system. Objectives of current work are thus to determine i) if the flow indeed reaches Mach 4 at the test section for the given wind tunnel wall configuration, ii) if the flow is fairly uniform upstream of the model, and iii) how the leading edge shock emanated from the model reflects from the wall and interacts with compression shocks and expansion waves generated by model support. The prevailing question is to see whether the flow expands over the model without the interference from the wind tunnel structure.

2. Numerical Method

The basic numerical algorithm follows Roe's flux-difference splitting (RFDS) method[2,3], although many ideas and features are adopted from flux-vector spilitting formulations of Warming and Beam[4], Pulliam and Steger[5], Pulliam and Chaussee[6], Steger[7,8], from conservative supra-chracteristics method (CSCM) of Lombard et al.[9-12], characteristic flux-difference splitting (CFDS) method of Yang et al.[13,14], among many others. Formulation for one-dimensional gasdynamics equations, and its extension to three-dimensional Navier-Stokes equations is described in detail in Refs. 15 and 16.

---

1) 국방과학연구소 책임연구원 (305-600, 대전시 유성우체국 사서함 35호 4-3-1).
2) 국방과학연구소 선임연구원 (305-600, 대전시 유성우체국 사서함 35호 4-3-1).

3. Results and Discussions

The results are presented in two parts: one for two-dimensional computations and the other, for three-dimensional computations. The 2-D case is performed first, since it provides the nature of flow physics faster than the 3-D problem.

3.1 Two-Dimensional Flows

The computation is performed from the throat where Mach number is 1 to the end of the diffuser which exhausts air into the open area. The entire computational domain is shown is Fig. 1 in the symmetry plane where locations of the throat, model, sting and the model support are indicated. Strut is omitted for 2-D computations for simplification, causing some disparity between those of the 2-D and 3-D. Nevetheless, the 2-D results should reveal the flow structure and influence of model support block in the wind tunnel.

The domain is divided by two regions: the one is from the nozzle throat to the end of test section, the other is from expanded area to the end of the diffuser section. The first region is discretized by 184x65 grid points, and the second, by 154x84. The grids are clustered densely normal to the wall as is apparent from Fig. 1. The computational grids between the first region and the second region are overlapped by a grid cell where the computed solutions exchange data after every iteration. The flow variables at the nozzle throat area are obtained from stagnation values at stroage tank and frozen throughout the computation. The values at the throat are: Mach = 1, Static pressure P = 105.6 (psia), Temperature T = 456.5 °R, Reynolds number per unit length = 5.3×10^7.

The rest of the field is started with a small, non-zero velocity with ambient pressure and density. This is done to capture the transient flow structure as the flow Mach number increases over the model and model support area. As the flow accelerates through the test section and the pressure expands, flow pattern over the model support area begins to exhibit a weak compression shock at the compression corner of model support.

At early stage, a weak normal shock is formed on the model support compression corner and then a leading edge shock begins to emerge from the model nose tip. When the flow upstream of the model has become nearly uniform Mach 4, the shear layer over the model support area has become thinned out and complex shock interaction structures appear as shown in Fig. 2 where interactions of compression shocks with reflected shocks are clearly captured. The strongly sheared viscous area in the wake of the backward-facing wall weakens the strength of the shock. The shock interaction pattern in Fig. 2 is re-sketched in Fig. 3 which seems to be reasonable in view of experimental shadow graphs taken for a similar test case.

Pressure contours over the test section area and to the end of the diffuser section are shown in Fig. 4 when the diffuser is fully open. Computed pressure distributions along the upper wind tunnel wall are compared in Fig. 5 between the current result (termed MFDS in the figure) and that of Rampant. The silhoutte of wind tunnel wall, model and model support block is sketched in the same figure to coordinate the location of pressure peaks with the model contours. The two computed curves show a good agreement overall; however, the pressure peaks over the narrow model block area and at the start of the diffuser section are quite different. This may be attributed to both the smearing of sharp corners by the current upwind method and the overshoot in the Rampant code in the absence of viscous shear layer at the wall.

3.2 Three-Dimensional Flows

3.2.1 Grid Structure

The computational domain is divided into five regions and shown in Fig. 6. Each of the five regions has the following number of grids for the total of 382,344 points: 34x58x60, for grid 1, 10x66x62 for grid 2, 24x66x60 for grid 3, 14x58x60 for grid 4 and 18x58x76 for grid 5, representing the number of grids in

ξ, η and ϕ coordinates. In the computational space ξ, η and ϕ are also replaced by J, K and L indecies.

The main flow is in the ξ or J direction, while η (K) and ϕ (L) coordinates are from wall to wall in each of J=constant plane. However, only the quarter of computational domain is solved invoking symmetry constraints at L=1 and K=1 planes. In Fig. 6, the vertical plane corresponds to L=1 plane while the horizontal plane represents K=1 plane.

3.2.2 Data Exchange

Although the five grids do not coincide at the interfaces of adjoining grids, the two planes are made coincident; that is, only two-dimensional interpolation is needed instead of three-dimensional one at the interface between two neighboring grids.

3.2.3 3-D Results

The convergence characteristics of 3-D solutions is shown in Fig. 7 as a time history of wall pressure values at two different locations: P_1 corresponds to the mid-plane of upper wall at the model support block area (J=6 at Grid 3) and P_2 at the wake section of the block (J=6 at Grid 4). The characteristic time represents accumulation of computational time increment non-dimensionalized by reference values. After quickly dropping to approximate steady state values, flow structure and contours would remain the same with minor variations near exit planes. Figure 8 shows Mach contours at two symmetrical planes along the wind tunnel main flow direction. The horizontal plane corresponds to K=1 plane ($\eta = constant$), while the vertical plane, to L=1 plane ($\phi = constant$). It shows that the heavy load is levied upon the frontal area of the model support block which holds the sting. Since the cross-sectional area becomes minimum over the model support block with the insert, oblique shocks merge in the region. It is speculated during the experiment with the current model at an angle of attack when fins are attached to the model body, those oblique shocks form a normal shock at the insert throat area. Figure 9 presents pressure contours in the K=1 plane, corresponding the horizontal plane in Fig. 8. They reveal shock formations at the nose section of the model, compression waves over the slope of the sting and a strong compression shock over the shoulder of model block and their interactions with reflected shocks from the wind tunnel side wall. Although there is some discrepancy between the 2-D geometry and that of 3-D, overall they exhibit good similarity between the two flow patterns; the discrepancy being mainly from omission of insert and the way the wind tunnel walls are modeled.

4. Concluding Remarks

Current work describes interference among projectile model, Mach 4 wind tunnel wall and model support to illuminate the flow pattern in the vicinity of the model and model support area. Work is reported here on a two-dimensional flow behavior at the mid-plane and then fully three-dimensional computation with more realistic representation of wind-tunnel second throat area.

Both 2-D and 3-D computations show a normal flow passage over the test model, reaching a uniform Mach 4 flow upstream of the model. Flow pattern in the downstream of the test model becomes complicated due to oblique shocks and their interactions among them. The current work captures these complex shock pattern over the model support block, though the shock formations are somewhat smeared with the flux-difference splitting upwind method, also due to sparse grid resolution in the flow direction. Despite successful results capturing complicated wall/shock interactions, the work still failed to capture the formation of stronger normal shock either in the base of the sting area or near the insert area observed during experiment. This is mainly attributed to not adquately modeling the downstream diffuser and the vertical stack which exhaust flow into the open air. The vertical stack would have increased the downstream wall pressure to close to the ambient pressure (0.139 when normalized by Pref.).

Nevertheless, the overall flow pattern is illuminated and is hoped to help understand flow physics on the way the reflected shock interfere with the supporting block system.

References

1. Lee, J. Y., "A Numerical Study of the Starting Process in a Hypersonic Shock Tunnel," Dissertation submitted to the Faculty of the Graduate School of The University of Maryland for the degree of Doctor of Philosophy, 1993.

2. Roe, P. L., "The use of Riemann problem in finite difference schmes," Lecture Notes in Physics, Vol. 141, 1981, pp. 354-359, Berlin, Springr Verlag.

3. Roe, P. L., "Approximate Riemann solvers, parameter vectors and difference scheme," J. of Computational Phisics, 43, 1981, pp.357-372.

4. Warming, R.F. and Beam, R. M.,"On the Construction of Implicit Factored Schemes for Conserbation Laws," Computational Fluid Dynamics, SIAM-AMS Proceedings, Vol. 11, 1978, pp.85-127.

5. Pulliam, T. H. and Steger, J. L. "On Implicit Finite Difference Simulations of Three-Dimensional Flows," AIAA 78-10, January 1978.

6. Pulliam, T. H. and Chaussee, D. S., "A Diagonal Form of an Implicit Approximate-Factorization Algorithm,", Journal of Computational Physics, Vol. 39, pp.347-363, 1981.

7. Steger, J. L. and Warming, R. F., "Flux Vector Splitting of the Inviscid Gasdynamic Equations with Application to Finite Difference Methods," J. Comp. Phys., Vol. 40., No.2, 1981, pp. 263-293.

8. Steger, J. L. "The Chimera Method of Flow Simulation," Workshop on Applied Computational Fluid Dynamics, August 1991.

9. Lombard, C. K., Oliger, J., Yang, J. Y. and Davy, W. C., "Conservative Supra-Characteristics Method for Splitting the Hyperbolic Systems of Gasdynamics with Computed Boundaries for Real and Perfect Gases," AIAA 82-0837, June 1982.

10. Lombard, C. K., Oliger, J., Yang, J. Y. "A Natural Conservative Flux Difference Splitting for the Hyperbolic Systems of Gasdynamics," AIAA 82-0976, June 1982.

11. Lombard, C. K., et al., "Multi-Dimensional Formulation of CSCM - An Upwind Flux Difference Eigenvector Split Method for the Compressible Navier-Stokes Equations", AIAA 83-1895, AIAA 6th CFD Conference, July 1983.

12. Hong, S. K., Bardina, J., Lombard, C. K., Wang, D. and Codding, W., "A Matrix of 3-D Turbulent CFD Solutions for JI Control with Interacting Lateral and Attitude Thrusters,"AIAA 91-2099, Sacramento, June 1991.

13. Yang, J. Y., "A Characteristic Flux Difference Splitting Method for Hyperbolic Systems of Conservation Laws," Ph.D. Thesis, Stanford University, June 1982.

14. Yang, J. Y. and Lombard, C. K., "A Characteristic Flux Difference Splitting for the Hyperbolic Conservation Laws of Inviscid Gasdynamics," AIAA 83-0040, Reno, Jan 1983.

15. Hong, S. K. and Jeon, H. J. ,"Computational Study of Supersonic Jet Impingement on Flat and Complex Surfaces," 25th Fluid Dynamics Conference, AIAA 94-2326, Colorado Springs, June 1994.

16. Hong, S. K., Ahn, H. K., Oh, S. J. and Cho, T. H., "Numerical Study of Model and Wall Interference in a Supersonic Wind Tunnel," 13th AIAA Applied Aerodynamics Conference, AIAA 95-1812, San Diego, June, 1995.

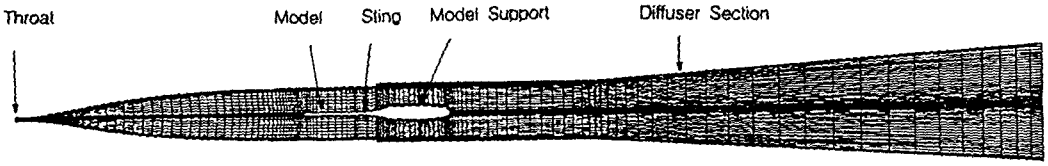

Fig. 1 Computational grid and wind tunnel configuration.

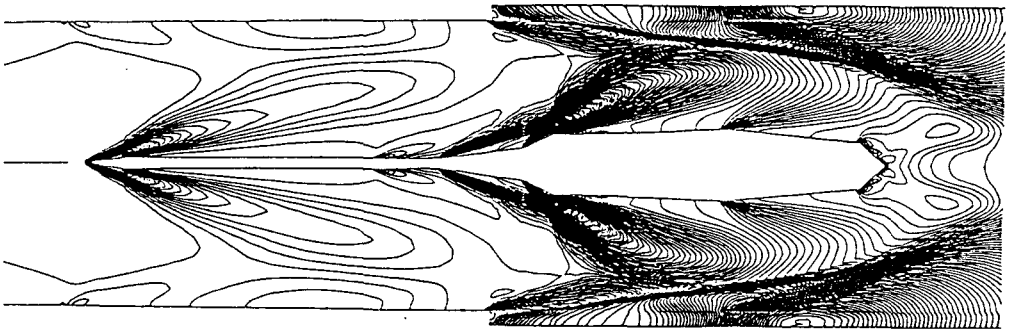

Fig. 2 Pressure contours over model and model support area when flow has fully developed over the model support area.

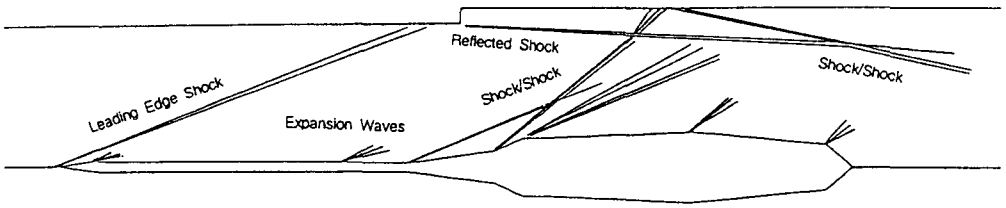

Fig. 3 Sketch of shock formations over model and model support Area.

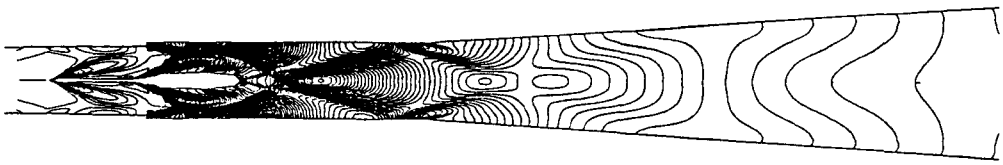

Fig. 4 Pressure contours over test section and diffuser (showing shock reflection and shock/shock interactions).

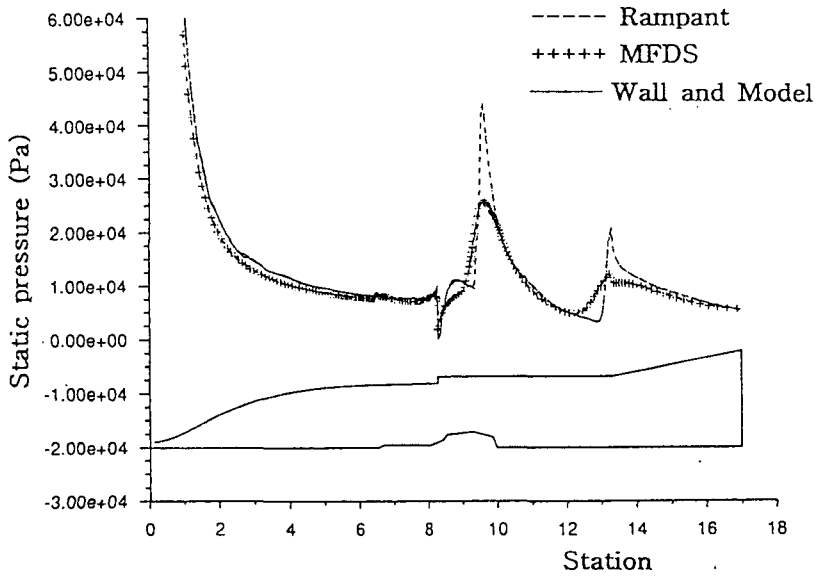

Fig. 5 Comparison of pressure distribution along W/T wall.

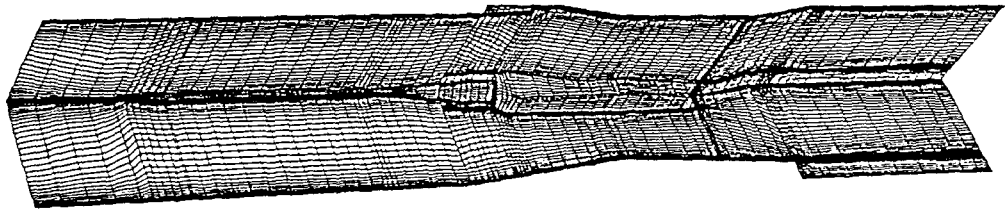

Fig. 6 Perspective view of computational grid along W/T mid-plane.

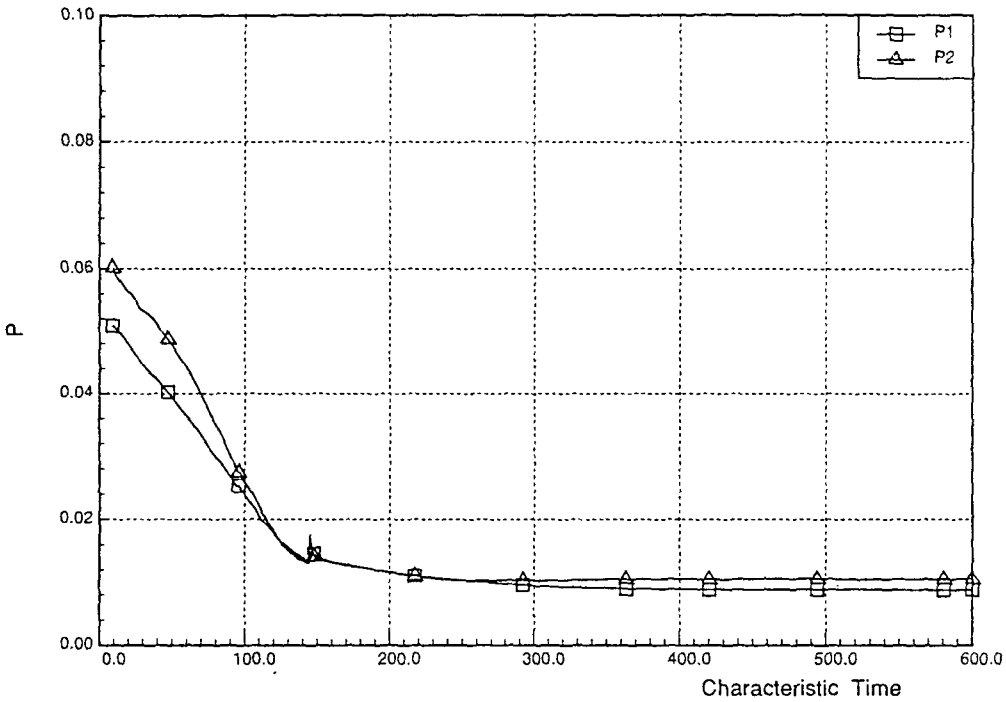

Fig. 7 Convergence of pressure at two selected wall locations.

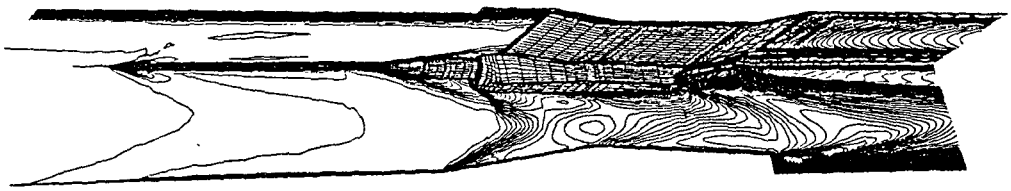

Fig. 8 Mach number contours in horizontal and vertical symmetry planes.

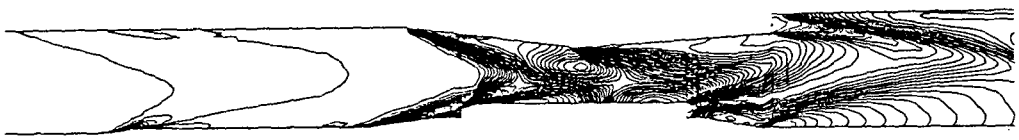

Fig. 9 Pressure contours in horizontal symmetry plane.